Mode I cracking versus dilatancy banding: Experimental constraints on the mechanisms of extension fracturing

A.I. Chemenda, Si-H. Nguyen, Jean-Pierre Petit, J. Ambre

Mode I cracking versus dilatancy banding: Experimental constraints on the mechanisms of extension fracturing

A. I. Chemenda,[1] S.-H. Nguyen,[1,2] J.-P. Petit,[3] and J. Ambre[1]

Received 15 November 2010; revised 18 January 2011; accepted 20 January 2011; published 7 April 2011.

[1] Fractures or discontinuities perpendicular to the least stress σ_3 were generated in a synthetic rock analogue (granular, frictional, cohesive, and dilatant) material in axisymmetric extension tests. These fractures are of two types defined by the mean stress σ. When σ is very small, the fractures form through the mode I cracking at tensile σ_3 equal to the material tensile strength. The fracture walls have smooth surfaces. At higher σ, these surfaces become rougher, with the topography features forming faint or delicate plumose patterns. The amplitude of the plumose topography increases with σ. The axial stress σ_3 at fracturing reduces in magnitude and changes in sign with the σ increase. Thus σ_3 orthogonal discontinuities can form at compressive σ_3. SEM observations show that these discontinuities are deformation localization bands where the material is characterized by the heterogeneous decohesion and volume and porosity increase due to dilatancy. The band thickness is several grain sizes. At formation, the bands are not opened, so they are not mode I fractures. They become fractures with plumose fractography after the separation of the sample parts along the band. The formation mechanism of these discontinuities or fractures is not completely clear, but it is suggested that it represents a running constitutive instability in the form of dilatancy banding (with further σ increase the bands become inclined to σ_1, i.e., shear). The similarity between the experimentally generated plumose surface fractures and natural joints is discussed, and it is suggested that they can be formed as propagating constitutive instabilities.

Citation: Chemenda, A. I., S.-H. Nguyen, J.-P. Petit, and J. Ambre (2011), Mode I cracking versus dilatancy banding: Experimental constraints on the mechanisms of extension fracturing, *J. Geophys. Res.*, *116*, B04401, doi:10.1029/2010JB008104.

1. Introduction

[2] The mechanism of quasi-brittle fracture/rupture remains one of the central problems in different domains of material science/mechanics including geomechanics. There are basically two approaches to this problem. The most developed one is the fracture mechanics based on the Griffith energy balance criterion that defines the stability condition of the preexisting crack (Griffith flaw) [e.g., *Lawn*, 1993]. This theory allows the stability criterion to be expressed in terms of one parameter (the stress intensity factor or energy release rate or J integral) as long as the size of the near crack tip yield/process zone (PZ) is small compared to other geometric dimensions of the problem. In many applications this condition is not met. The growing fracture advances into previously inelastically strained (hence hardened or softened) areas. This affects the fracture behavior and makes it essential to consider the true incremental and path-dependent nature of inelastic stress-strain relations [*McClintock and Irwin*, 1965; *Rice*, 1968].

[3] Usually, the inelastic response is only taken into account through the use of fracture energy. This energy (which is equivalent to but very different from a surface energy) is calculated from the nominal stress-strain curves measured experimentally [e.g., *Hillerborg et al.*, 1976; *Petersson*, 1981; *Wong*, 1982; *Bažant and Planas*, 1998]. Although this approach provides more realistic results than linear elastic fracture mechanics (LEFM) [e.g., *Bažant and Planas*, 1998], the fracture energy is not a material constant any longer and strongly depends on the geometry (including size) of the structure or specimen and the entire loading path. This induces uncertainties related notably to the scaling problem [e.g., *Bažant and Planas*, 1998; *Van Mier*, 1997].

[4] Another view of the failure of materials different from fracture mechanics is the formation of deformation localization bands, whose onset in quasi-brittle rocks can be considered as corresponding to the inception of rupture. The mechanism of this phenomenon is not totally understood. The most pertinent and developed concept is a constitutive (or material) instability resulting in the deformation bifur-

[1]Géoazur, Université de Nice-Sophia Antipolis, Valbonne, France.
[2]Now at Department of Project Management, Academy of Managers for Construction and Cities, Ministry of Construction, Hanoi, Vietnam.
[3]Géosciences Montpellier, Université Montpellier 2, Montpellier, France.

0148-0227/11/2010JB008104

cation and formation of localization bands [*Rice*, 1973, 1976; *Rudnicki and Rice*, 1975]. The instability can result from the continuous or discontinuous evolution of the hardening modulus with deformation. The latter leads to the formation of the localization band networks with the material outside the bands undergoing elastic unloading [*Chemenda*, 2007, 2009]. The bifurcation approach is supposed to predict the inception of rupture in a "natural way" as a result of progressive material damage/microfracturing, which is itself described in terms of the evolution (whether smooth or not) of macroconstitutive parameters.

[5] Rock mechanics tests generally seem to confirm the results of bifurcation analysis (see *Vardoulakis and Sulem* [1995] and *Bésuelle and Rudnicki* [2004] for a review). This approach provides a useful framework for analyzing the initiation of macrofailure in geomaterials but gives no indication on the evolution of this process toward large inelastic deformation. At such deformation, the localization bands appear as propagating (crack-like) features [e.g., *Reches and Lockner*, 1994]. This suggests some analogy with fracture mechanics and the need to extend the deformation localization theory beyond bifurcation analysis toward the connection with crack-type fracture mechanics. It is not quite clear as yet how to provide such a connection.

[6] The above schematic presentation of the state of the art of mechanics of quasi-brittle rupture shows difficulties encountered by both end-member approaches in which fracture/rupture is viewed correspondingly as a propagating crack or resulting from a material instability. The most difficult and probably most important area for applications is a transition between these two. In spite of a large amount of enlightening experimental results on rocks and other materials with similar properties (soils, cements, ceramics, glass, ice), some of which are cited in this paper, there still remains a critical lack of sufficiently precise and detailed experimental information (including mechanical, microstructural, and fractographic data) necessary for deeper understanding of the rupture processes.

[7] With the presented problems in mind, we report in this paper the results from the axisymmetric extension tests on an "ideal" synthetic granular, frictional, cohesive, and dilatant physical rock analogue material GRAM1 [*Nguyen et al.*, 2011]. We concentrate on this loading configuration because it provides the most direct and easiest way for generation of extension (other terms are tension and tensile) fractures, which are the most frequent in different materials and above all in geological structures, where they are called joints [e.g., *Pollard and Aydin*, 1988; *Mandl*, 2005].

[8] After concise presentation of the GRAM1 material and experimental techniques (described in detail by *Nguyen et al.* [2011]), we focus in this paper on the conditions of formation, fractography, and microstructure (scanning electron microscope (SEM) observations) of the extension fractures generated in GRAM1 experiments. On the basis of these data we discuss the fracturing mechanism and argue that it changes with the mean stress σ from mode I (opening mode) cracking to running constitutive instability in the form of dilatancy banding. This seems to correspond to the transition between the two end-member rupture mechanisms indicated above. We then discuss the origin of the geological joints and argue that they can be formed (initiated) as dilatancy bands.

2. GRAM1 Material and Experimental Procedure

2.1. GRAM1

[9] Granular Rock Analogue Material 1 (GRAM1) samples are fabricated from a finely ground powder of TiO_2 with the average grain size of ~0.3 μm. The powder is subjected to the hydrostatic pressure of P^{fabr} = 2 MPa at which the grains are bonded one to another. An extensive program of GRAM1 stress-strain measurements in axisymmetric compression and extension tests at different confining pressures P below P^{fabr} show that this material has frictional, cohesive, and dilatant properties very similar to those of hard rocks [*Nguyen et al.*, 2011]. GRAM1 produces the same macrofailure features as rocks, from very brittle splitting to shear fractures/bands and compaction bands with P increase, but is about 2 orders of magnitude less strong and less rigid than rocks. Therefore in describing GRAM1 properties and their comparison with rock properties, it is convenient to use dimensionless values of parameters having dimensions of stress. These parameters can be normalized by the uniaxial compression strength σ_c, which for GRAM1 is σ_c = 0.57 MPa. Below we will use both normalized and absolute parameter values.

[10] As for rocks, the GRAM1 elastic properties are almost independent from the loading conditions, while inelastic response, especially at high P, depends on these conditions. The normalized confining pressure $\tilde{P} = P/\sigma_c$ and mean stress $\tilde{\sigma} = \sigma/\sigma_c$ at the onset of brittle-ductile transition in GRAM1 under extension (here and below we omit the word "axisymmetric") are $\tilde{P}_{bdt}$ = 2.3 and $\tilde{\sigma}_{bdt}$ = 1.7. For Solnhofen limestone, $\sigma_c \approx 0.34$ GPa and σ_{bdt} under extension is σ_{bdt} = 0.56 GPa [*Heard*, 1960], and hence $\tilde{\sigma}_{bdt}$ = 1.6, which is very close to the above GRAM1 value. For GRAM1, $\tilde{\sigma}_{bdt}$ under compression is 1.7 times smaller than under extension. For Solnhofen limestone the difference is 2 times, which is again rather close to the GRAM1 data.

[11] At low $\tilde{P}$ (in brittle regime) the internal friction coefficient α defined as $\alpha = \partial\overline{\tau}^{pk}/\partial\sigma$ can be considered constant and the same for compression and extension conditions ($\overline{\tau}^{pk}$ is the peak Mises stress corresponding to the failure envelope). On the contrary, the cohesion k under compression is considerably larger than under extension. The dilatancy factor β reduces with P for both loading configurations, but under extension it is larger than under compression for the same $\tilde{\sigma}$.

[12] The GRAM1 Young's modulus is $E = 6.65 \times 10^8$ Pa, the Poisson's ratio is ν = 0.25, the internal friction coefficient is $\alpha \approx 0.6$, the dilatancy factor β for extension conditions varies from 0.4 at P = 0.4 MPa ($\tilde{P}$ = 0.7) to −0.2 at P = 1.3 MPa ($\tilde{P}$ = 2.3) corresponding to the brittle ductile transition, the porosity is 57%, and the density is 1723 kg/m^3 (its variation from sample to sample does not exceed 1.2%).

2.2. Experimental Procedure

[13] We resume here a detailed description of the work of *Nguyen et al.* [2011]. The tested samples were first hydrostatically loaded to pressure P and then unloaded in

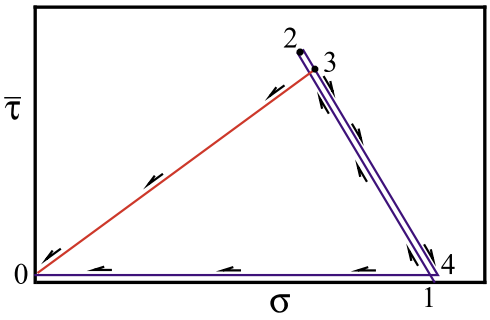

Figure 1. Loading paths applied in the presented tests: path 1, 0–1–2–3–4–0; path 2, 0–1–2–3–0.

the axial direction at $P = const$. The unloading was stopped at a certain deformation stage after the failure onset or just at the onset, which was detected by the stress jump on the stress-strain curves. After the test was stopped, the samples were unloaded following one of the two paths (Figure 1) in order to investigate a possible influence of unloading conditions on the fractography and microstructure. In the case of path 1, the fractured sample was first vertically loaded to the initial hydrostatic state and then was unloaded hydrostatically to $P = 0$. Path 2 was applied in the tests where the final axial stress σ_{ax}^{pk} was either tensile or slightly compressive. In the latter case, σ_{ax}^{pk} was kept constant and P was reduced to the value of this stress. Then complete unloading was done hydrostatically. When σ_{ax}^{pk} was tensile, it was increased to slightly positive (compressive) value and maintained constant during P reduction to this value. Complete unloading was done hydrostatically.

[14] Both cylindrical and dog bone–type samples were used [*Nguyen et al.*, 2011]. The dog bone–samples were used in the tests where the tensile axial stress was required (i.e., in low P tests).

3. Results

[15] Below we present results of (1) mechanical response of the material during fracturing using stress-strain curves, (2) fracture surface topography (fractography), and (3) microstructure of the rupture zones (SEM data). Most of the tests used were reported by *Nguyen et al.* [2011] and conducted according to loading path 1 in Figure 1. In this paper we add data from six more tests (Table 1) conducted with paths 1 and 2.

3.1. Fracture Conditions, Orientation, and Fractography

[16] Figure 2 shows examples of samples fractured in extension tests at different P. As is shown in Figures 2 and 3, the angle ψ between σ_1 and the fractures strongly depends on P or σ ($\sigma_1 > \sigma_2 > \sigma_3$ are the principal stresses; the compressive stress is positive). At $P < 0.7$ MPa ($\sigma < 0.48$ MPa; $\tilde{\sigma} < 0.84$) the fractures are perpendicular to the axial stress ($\psi = 0°$). Their formation is accompanied by acoustic emissions (sharp snapping noises) evidencing the dynamic brittle failure of the material. The dynamic character of failure can also be deduced from the stress-strain curves in Figure 4, showing the stress jump after reaching the minimal axial stress. Figure 4 shows also that the "brittleness" of the material response at fracturing reduces with P increase.

[17] After extracting the unloaded sample from the pressure cell and the jacket, the fracture appears at the sample surface as a hardly visible, very thin discontinuity. Manual separation of the sample parts along the discontinuity reveals its surfaces/walls. The surfaces of σ_3 orthogonal discontinuities/fractures exhibit faint and delicate ridges and troughs forming a plumose topography complicated with steps (Figures 5 and 6) appearing at relatively high pressures (Figures 5d–5f and Figure 6). This small-scale topography becomes less expressed with P reduction and disappears completely at $P < \sim 0.2$ MPa ($\sigma < 0.11$ MPa; $\tilde{\sigma} < 0.2$) (Figures 5a and 5b).

[18] Figure 7a shows a fracture surface with two distinct parts, one smooth and the other decorated with a plumose pattern. This fracture was created in two stages. The first one was the same as in the above experiments: The sample was subjected to axial extension at $P = 0.6$ MPa. After unloading, the surface of the fractured sample showed a trace/discontinuity that did not cut through the whole sample. Then the sample parts were separated manually in an approximately axial direction, which resulted in the fracture surface shown in Figure 7a. The part of this surface with a plumose feature corresponds to the discontinuity seen at the sample surface after unloading, and the smooth part was formed during the manual extension at $P = 0$ due to the fracture propagation from the discontinuity front.

[19] The axial stress $\sigma_{ax}^{pk} = \sigma_3^{pk}$ (stress peak/extremum) at σ_3 orthogonal fracturing reduces with P reduction from positive values (compression) at $0.6 < P < 0.7$ MPa to negative values at $P < 0.6$ MPa and reaches almost stationary value $\sigma_{ax}^{pk} = -\sigma_t$ at $P < 0.2$–0.4 MPa (Figure 3); $\sigma_t = 0.07$ MPa is the GRAM1 tensile strength. At $P > 0.7$ MPa, the fractures become inclined to σ_1, with the inclination angle ψ growing with P (Figure 3; see *Nguyen et al.* [2011] for more data on variation of ψ with σ).

3.2. Microstructure

[20] The most intriguing result is that the σ_3 orthogonal discontinuities can be formed at small (much lower in magnitude than σ_t) tensile and even at compressive $\sigma_3 = \sigma_{ax}^{pk}$. In the latter case (at $P \geq 0.6$ MPa), these discontinuities (failure features) do not open at formation, but they open if axial extension of the sample continues after fracturing. To access the structure of these discontinuities before opening, we conducted tests at $P \geq 0.6$ MPa where extension was stopped just after or at reaching the stress extremum σ_{ax}^{pk}

Table 1. Mechanical Data From GRAM1 Extension Tests Conducted With Different Loading Paths

Test	$P = \sigma_1 = \sigma_2$ (MPa)	$\sigma_3^{pk} = \sigma_{ax}^{pk}$ (MPa)	σ^{pk} (MPa)	Loading Path
Ex-151	0.65	0.019	0.440	1
Ex-81a	0.65	0.006	0.435	1
Ex_JA_9	0.6	0.015	0.405	2
Ex_JA_10	0.6	−0.002	0.399	2
Ex_JA_11	0.6	0.001	0.400	2
Ex-JA_13	0.6	0.008	0.403	2

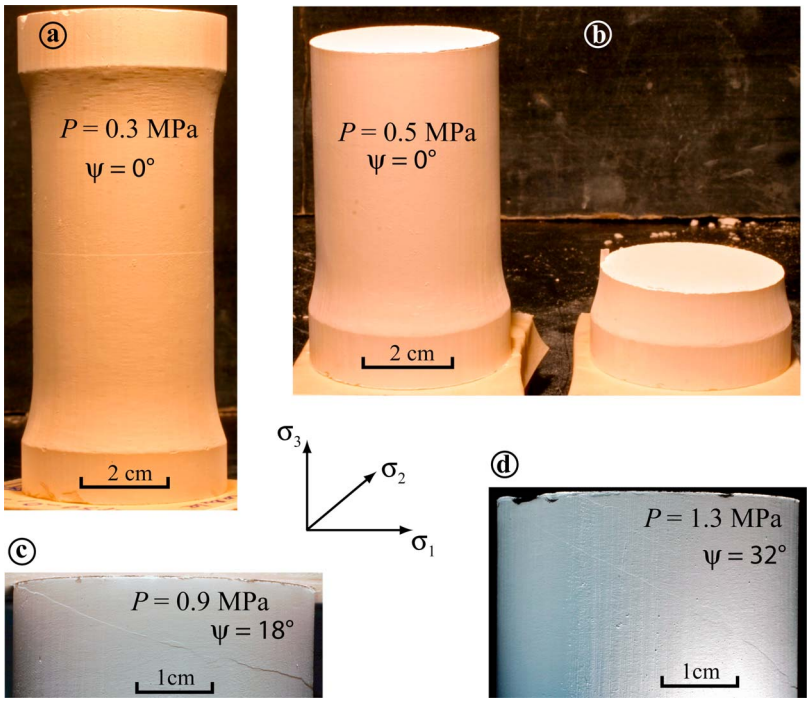

Figure 2. GRAM1 samples fractured in extension tests at different P: (a) test Ex–150; (b) test Ex–157; (c) test Ex–48; and (d) test Ex–a1 [from *Nguyen et al.*, 2011].

(the minimum of σ_{ax}), after which the sample was unloaded following either path 1 or 2 in Figure 1.

[21] After the removal of the jacket from the unloaded sample, a PVC tube was put around the sample (the internal diameter of the tube is somewhat larger than that of the sample). The space between the sample and the tube was filled with a low-viscosity epoxy resin which penetrated the pores both inside and outside the band. After the polymerization (solidification) of the resin, the sample was cut perpendicularly to the band and the section was carefully polished before observation. Figures 8c and 8d show the SEM images of such sections from two samples fractured at P = 0.6 MPa and unloaded following the different paths. The displayed structures were observed in many images of different parts of the band and cannot be induced by cutting/polishing procedures. At SEM scale, the discontinuities in

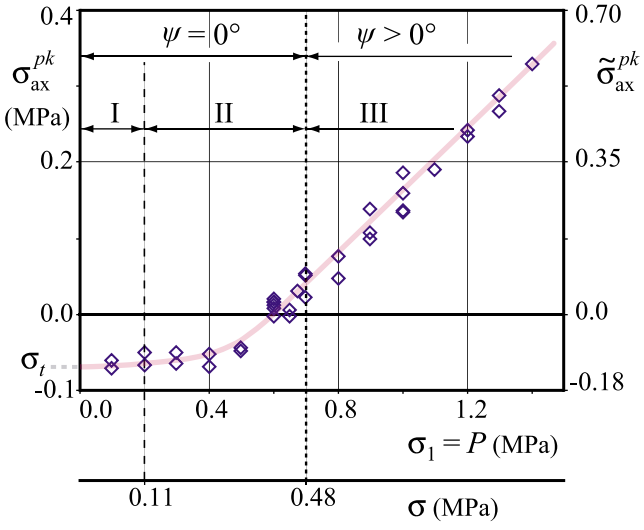

Figure 3. Axial stress peaks $\sigma_{ax}^{pk} = \sigma_3^{pk}$ and their normalized values $\tilde{\sigma}_3^{pk}$ versus $P = \sigma_1$ and σ. Numerals I, II, and III are the domains of mode I fracturing (no plumose fractography), dilatancy banding (plumose fractography), and shear banding, respectively.

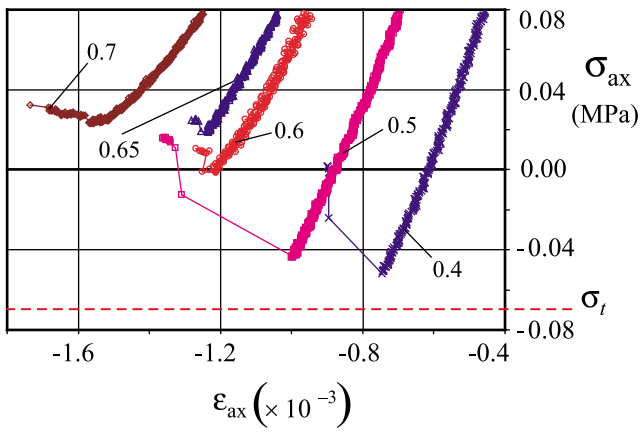

Figure 4. Axial stress σ_{ax} versus axial strain ε_{ax} in the vicinity of the fracturing or rupture point (σ_{ax}^{pk}) for different P indicated on the graph in MPa. P = 0.4 MPa (Ex–160); P = 0.5 MPa (Ex–157); P = 0.6 MPa (Ex_JA_10, Table 1); P = 0.65 MPa (Ex–151, Table 1); P = 0.7 MPa (Ex–58). All tests except Ex_JA_10 and Ex-151 are from *Nguyen et al.* [2011].

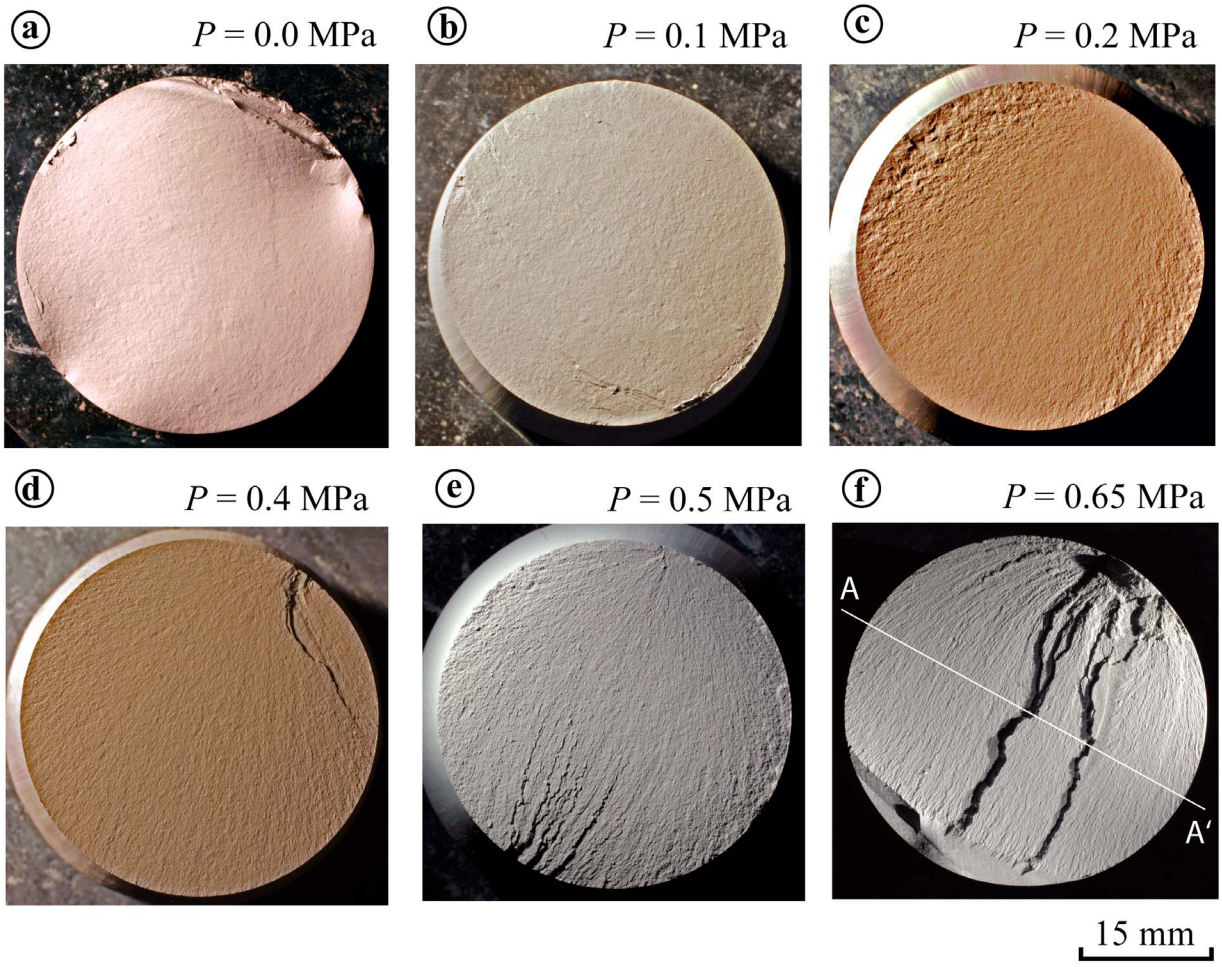

Figure 5. Surfaces of the σ_3 orthogonal fractures generated at different P: (a) test Ex–0; (b) test Ex–170; (c) test Ex–134; (d) test Ex–124; (e) test Ex–140; and (f) Ex–81a. AA′ in Figure 5f indicates the section shown on Figure 6.

both cases represent nonplanar, several-grain-thick bands of heterogeneously damaged material. The bands consist of voids of different shapes and sizes, zones of loose grains indicating decompaction/dilatancy, and bridges of apparently intact material. There is clearly neither an along-band progressive/monotonous evolution of the deformation/damage nor a progressive separation of the band (future fracture) walls. Above grain scale, there is no separation at all. The material within the band underwent partial heterogeneous decohesion and dilatancy defined by *Reynolds* [1885] as an inelastic volume/porosity increase of the material caused by its deformation (the inelastic volumetric and shear deformations are proportional, with the dilatancy factor β being the coefficient of proportionality). Dilatancy therefore defines a deformation and not a displacement/opening. Thus the deformation bands obtained in our experiments are dilatancy bands (because of the above definition, we use the term dilatancy instead of dilation). The micromechanism of deformation within the bands cannot be read directly from the SEM images, but the grain separation is obvious. Because of the nonplanar geometry of the bands at this scale, microshearing accommodated by grain sliding, translation and rotation is certainly present as well. All are distributed in

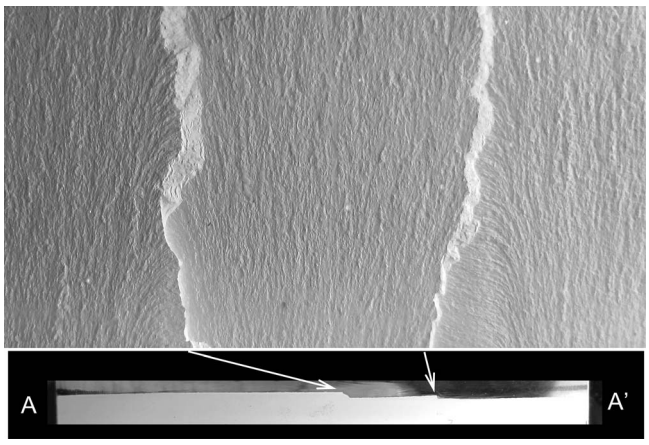

Figure 6. Close-up of a part of the fracture surface opposite to that shown in Figure 5f and the corresponding orthogonal section of the whole sample width (4 cm) along AA′. As in Figure 5f, one can see the steps between quasi-parallel segments of the fracture surface, which are practically orthogonal to the sample borders (seen on the section) and axis and hence to σ_3.

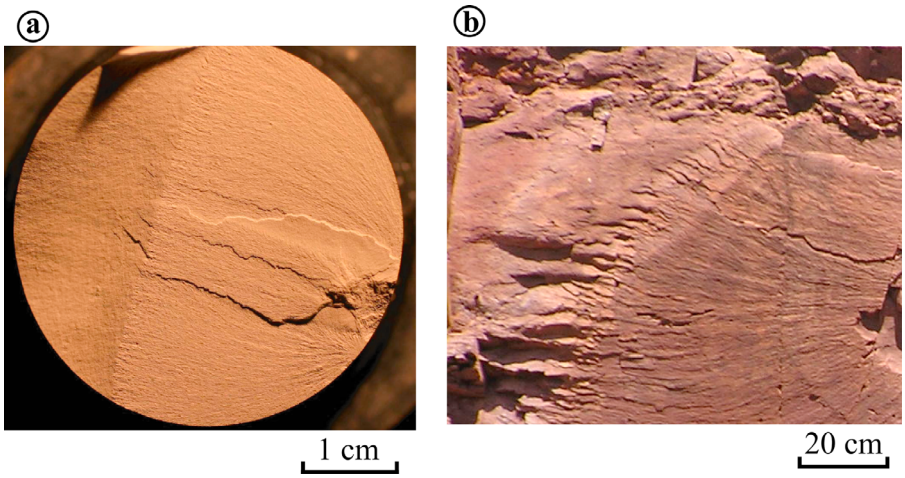

Figure 7. Fracture surfaces consisting of two parts, smooth and with plumose. (a) Fracture generated in two steps in GRAM1 sample (test Ex–75). The first step is dilatancy banding in the extension test at $P = 0.6$ MPa, resulting in the formation of the plumose bearing part of the surface. The second step is a manual subaxial extension of the sample at $P = 0$, resulting in the formation of the smooth part of the surface. (b) A joint surface in the Permian pelites of the Lodève basin (southern France).

a complex manner in three dimensions and result in the volume/porosity increase.

[22] As far as the fractures formed at tensile σ_{ax}^{pk} are concerned, their pristine (prior to opening) microstructure cannot be preserved with the used "multiple-freedom-degree" upper platen of the loading device located between the upper end of the sample and the load frame (piston). It is designed so as to avoid/reduce the possible deviation of the sample stress-state from the axial symmetry that can occur during the deformation. The platen element in contact with the sample is not fixed to the load frame in a rigid manner [*Nguyen et al.*, 2011, Figure 3b]. This allows the rebound (rapid uplift) of the part of the sample located above the fracture during dynamic rupture, which results in the fracture opening. This effect is seen in the graphs in Figure 4. When $\sigma_{ax}^{pk} < 0$, the rupture is followed not only by the $|\sigma_{ax}|$ drop but also by an abrupt increase in $|\varepsilon_{ax}|$ due to the fracture opening. When $\sigma_{ax}^{pk} > 0$ (i.e., at $P \geq 0.6$ MPa), the rebound is impossible. To remove this effect in the tests with tensile σ_{ax}^{pk}, the upper platen should be fixed to the piston in a rigid manner, but in this case the stress-strain state of the sample will be less uniform. Thus we do not have direct access to the microstructure of the fractures formed at $\sigma_{ax}^{pk} < 0$, but we can observe their fractography, which bears important information about the fracture process.

4. Discussion of Possible Formation Mechanisms of the Obtained Fractures

[23] It is logical to suppose that the two revealed fractographic types of σ_3 orthogonal fractures correspond to different formation mechanisms.

4.1. Smooth-Surface Fractures

[24] According to Figure 3, the failure condition for this fracture type is $\sigma_3 \approx -\sigma_t$ and it does not seem to depend on the two other principal stresses (domain I in Figure 3), which suggests a mode I mechanism. This conclusion agrees with the *Griffith* [1924] theory (different from the theory of the same author discussed in section 1), which considers that the fracture occurs when the tensile stress along the boundaries of representative (for this material) randomly oriented microcracks reaches a certain critical value σ_{tip} (this value defines the macrotensile strength σ_t). The orientation of the resulting macrofracture is defined by the orientation ψ of a "favorable" microcrack for which σ_{tip} is maximal for a given stress state (ψ is defined in the far-field principal stress coordinates). Griffith obtained that at $\sigma_1 < 3\sigma_t$, $\psi = 0$, i.e., that the favorable microcrack is orthogonal to the tensile σ_3 and propagates in its own plane, hence in mode I. This agrees well with our experiments where the smooth-surface fractures were generated only at $\sigma_1 < 0.2$ MPa $\approx 3\sigma_t$ ($\sigma_t = 0.07$ MPa).

4.2. Plumose-Surface Fractures

[25] At $\sigma_1 > 3\sigma_t$ (equivalent in our experiments to $\sigma_3 > -\sigma_t$ and corresponding to $P > 0.2$ MPa, Figure 3), the favorable microfractures become oblique [*Griffith*, 1924]. They should therefore accommodate shear displacement, "activate" internal friction and complex interaction of different microcracks whether favorable or not. Failure of material in these conditions can no longer be considered as a propagation of a single/isolated crack but should be addressed in terms of a theory describing the collective behavior of microfractures, voids, and grains. Plasticity theory is of this type.

[26] This general reasoning (which is not new at all) finds clear confirmation in our results. There is as yet no clear understanding of how the interaction of the above small-scale processes produces macrofailure, but we see the result of this process: It is a narrow dilatancy band with the internal structure bearing traces of all the processes described above (Figures 8c and 8d). Although dilatant, the band is initially closed and, moreover, can be formed under compressive stress perpendicular to the band. Therefore it is

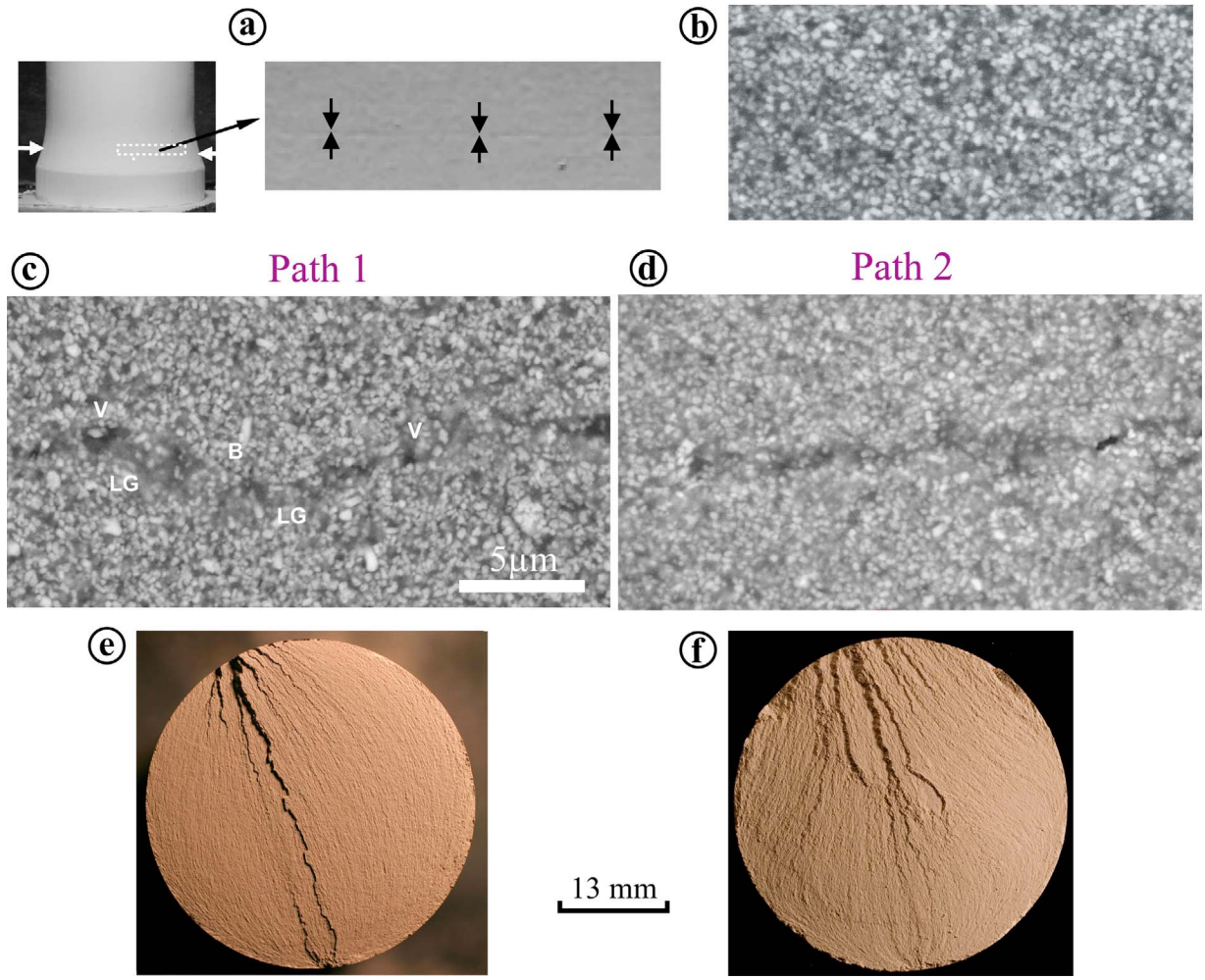

Figure 8. (c and d) Scanning electron microscope (SEM) images of the dilatancy bands and (e and f) optical views of the plumose surfaces formed at $P = 0.6$ MPa in GRAM1 samples unloaded along different paths. (a) General view of the fractured sample and aspect of the band/fracture. (b) SEM image of the intact (undeformed) GRAM1 material. The scale indicated in Figure 8c is the same for all SEM images. At this scale, the dilatancy bands are formed by an alignment of voids (V), loose grain zones (LG) where the decompacted grains are surrounded by the resin (blurred grey background around the grains), and by zones (bridges, B) of apparently intact material as is shown in Figure 8c. The band thickness is several grain diameters. Figure 8c shows test Ex-156 (path 1); Figure 8d shows test Ex_JA_13 (path 2); Figure 8e shows test Ex-123 (path 1); and Figure 8f shows test Ex_JA_11 (path 2).

not really a fracture (in the sense that there are no distinctive/clear cut fracture walls). After its opening, no direct traces of the band remain (except maybe some undetectable amount of the powder shed on the table) whose thickness in GRAM1 does not exceed a few microns. The indirect trace of the band is the plumose relief of its boundaries (fracture walls), which is defined by the material decohesion pattern (apart from the plumose features there is no apparent difference between the fractures of both types at sample scale).

[27] The plumose patterns (presence of the initiation points and the diverging network of delicate ridges and grooves stemming from them) provide some information about the band/fracture kinematics and dynamics abundantly discussed in literature (notably geological in application to the joints) [e.g., *Bahat*, 1991]. These patterns show in particular that the band is a σ_3 orthogonal propagating feature (the propagation/failure is dynamic as indicated above). This would suggest the mode I type crack mechanism, but this is false, as the band was not opened at formation. The most likely mechanism is a kind of constitutive instability similar to that analyzed by *Bigoni and Hueckel* [1991], *Ottosen and Runesson* [1991], *Perrin and Leblond* [1993], and *Issen and Rudnicki* [2000] and resulting in formation of σ_3 orthogonal localization (splitting or dilation) bands. In the theoretical bifurcation analysis, the localization bands are assumed to be initiated throughout the whole body, independent of whether it is infinite [*Rudnicki and Rice*, 1975] or finite [*Chemenda*, 2007]. Such an idealization is imposed by the mathematical complexity in analyzing more complex/adequate deformation patterns, and in any case the analysis applies only to the onset of localization banding when the inelastic deformation

(damage) is infinitesimal. What we are normally able to observe in the laboratory experiments is the result of post-bifurcation evolution of deformation when it was finite and not homogeneous. This deformation can be modeled in dynamic numerical models. Such models [*Chemenda*, 2007, 2009] confirm on the one hand the predictions of the bifurcation theory regarding the conditions of the bifurcation onset, orientation, and average spacing of the bands. On the other hand, they show that the deformation bands are not continuous even at the onset in the homogeneous stress-strain field and that they can propagate with the increase in deformation similar to cracks [*Chemenda*, 2011].

[28] What suggests to us that this approach based on the plasticity theory is adequate to tackle the problem of material failure though the dilatancy banding that appears as a running constitutive instability? There are three arguments: (1) The failure criterion for GRAM1 at $P > 0.2$ MPa (including at $0.2 < P < 0.7$ MPa when the plumose-bearing, σ_3 orthogonal macrofailure structures/dilatancy bands are generated) depends on all stresses (domains II and III in Figure 3). (2) The thickness of the obtained dilatancy bands (several grain sizes) is approximately the same as for other better understood types of localization bands (shear and compaction) whose formation is usually analyzed within the frame of plasticity and bifurcation theories (see *Vardoulakis and Sulem* [1995] and *Bésuelle and Rudnicki* [2004] for a review). (3) The importance of the dilatancy property and its impact on the band orientation which in rock experiments is qualitatively the same as that predicted from the deformation bifurcation theory: ψ increases with reduction of the dilatancy factor (increase in P) [e.g., *Wong et al.*, 1997; *Bésuelle*, 2001; *Sulem and Ouffroukh*, 2006]. Quantitatively, however, the predictions are known to be different (sometimes considerably so) from the experimental data. This is also true for our data: The β value for GRAM1 does not exceed 0.5 [*Nguyen et al.*, 2011], whereas the continuous bifurcation analysis [*Issen and Rudnicki*, 2000] predicts that for the dilatancy banding to occur, β should be more than 1.2. This may suggest that the used simple/general two-invariant Drucker-Prager constitutive formulation with stress independent constitutive parameters and/or the above continuous bifurcation analysis are not completely adequate. In any event, there is no other theory predicting (at least qualitatively) the variation of ψ with β or σ. The classical fracture mechanics including its basic/elementary part, LEFM even does not include such important rock property as dilatancy. According to this theory, the fracture tends to be orthogonal to σ_3 whatever the other stress values and their ratios or the material properties such as internal friction and dilatancy. This clearly does not correspond to the presented (and many other) experimental data except for the opening mode fractures with smooth surfaces forming at very low σ as indicated above.

4.3. What Determines the Roughening of the Fracture Surface and the Change of the Fracture Mechanism With Increasing σ?

[29] This change in the relief of σ_3 orthogonal fractures very clearly demonstrated in the presented experiments (Figures 5 and 7a) also contains important information on the mechanics of the failure process. It is not clear yet how to decode it, but it appears certain that this process and the resulting plumose relief are related to the regime of the constitutive instability. As shown by both theoretical and numerical analyses by *Chemenda* [2007, 2009], this instability can result in different thicknesses and shapes of the localization bands depending on the stress-state and constitutive parameters and first of all on the hardening modulus h and β [*Chemenda*, 2009] (α can be considered constant in the brittle domain as indicated above). The bands can have linear or zigzag shapes with different wavelength and amplitude depending again on the parameters and in particular on β. This parameter is not only strongly pressure dependent (which may be a cause of the pressure dependence of the obtained results/fractography). It also varies with the accumulated inelastic deformation $\overline{\gamma}^p$ (initially large, positive β reduces with $\overline{\gamma}^p$ as both rock mechanics [*Sulem and Ouffroukh*, 2006] and GRAM 1 [*Nguyen et al.*, 2011] data show). The dynamics of dilatancy banding should be related to the evolution of β and other constitutive parameters with $\overline{\gamma}^p$. Understanding this relation requires further combined experimental, theoretical, and numerical investigations.

[30] It is important that neither fractographic patterns nor dilatancy band microstructures depend on the loading or unloading path of the sample after its rupture (Figure 8). In the case of path 1 (Figure 1) the damaged material within the band is subjected first to axial compression before hydrostatic unloading. This compression does not induce further damage/inelastic deformation within the band, as it results in the reduction of the deviatoric stress and hence in the shift of the stress state from the yield/failure surface (where it was at the moment of rupture) inside this surface (toward the hydrostatic axis) where only elastic (reversible) response is possible. In the path 2, the stress state approaches the hydrostatic axis due to the reduction of P at constant σ_{ax}, but the result is the same: no inelastic deformation.

5. Comparison With Geological Joints

[31] The fractures of the second type (dilatancy bands) obtained in the presented experiments are very similar to geological joints. The similarity is expressed first of all in the plumose topography (Figures 5, 6, 7a, and 10) and the orientation of experimental and geological joints (both are orthogonal to σ_3). This similarity suggests that the natural joints with plumose fractography have been initiated as dilatancy bands and not as mode I fractures as is commonly considered in geological literature [e.g., *Pollard and Aydin*, 1988]. Such a hypothesis could have more weight if it could be proved that the relief of joints formed in natural conditions shows the same sensitivity to σ as was demonstrated in GRAM1 experiments. Finding direct proof is difficult, as we do not know the exact conditions in which a given natural fracture has been generated. Indirect evidence is given in Figure 7, which shows surfaces of natural and experimental joints having two distinct parts. We know the origin (described above) of these parts in GRAM1 samples. It suggests the following formation scenario for the natural joint in Figure 7b: The plumose-bearing part of this joint may have formed through the dilatancy banding at depth (at high σ) and the smooth part may have resulted from mode I crack propagation during late stages of exhumation

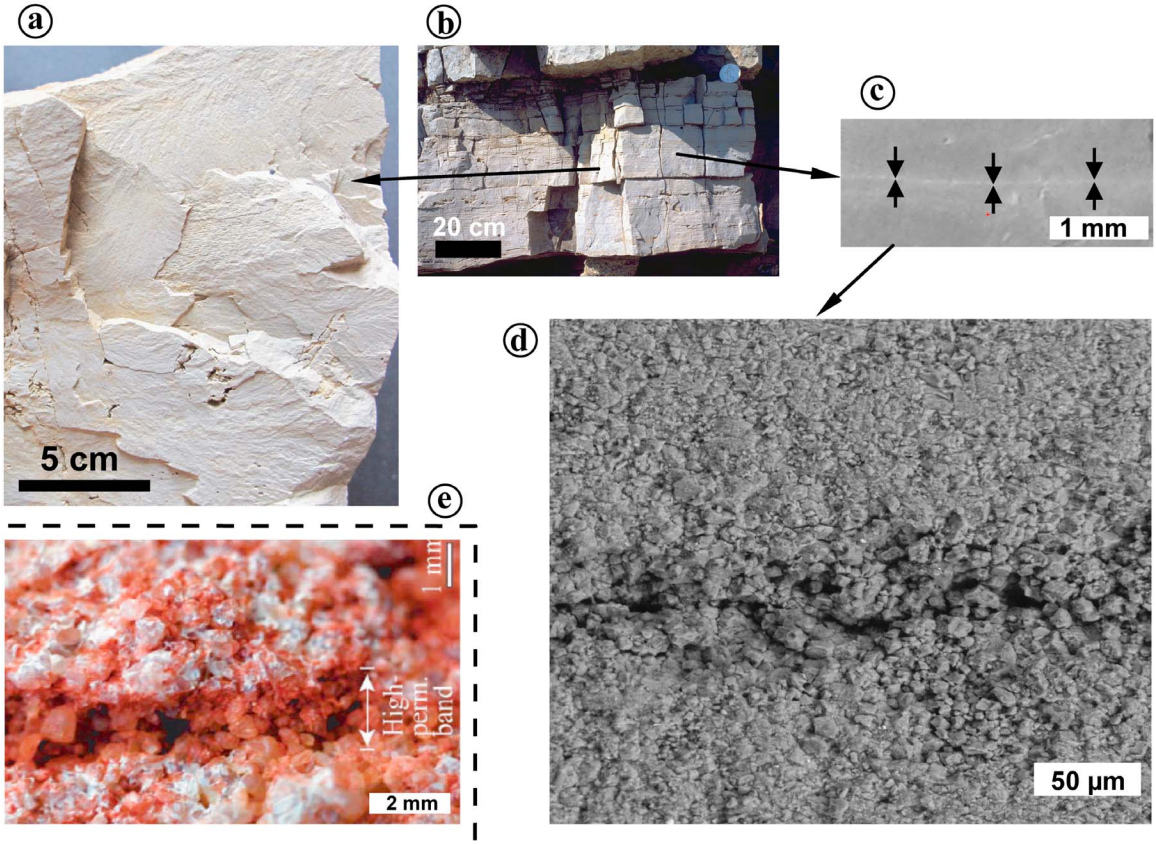

Figure 9. Natural dilatancy bands. (a) Aspect of plumose features on an open joint. (b) Outcrop in the densely jointed dolomicrites ("cubic dolomite") of the tabular Hettangian layers of the Larzac Plateau boarder (southern France). (c) Aspect of the trace (on a sawn and polished surface) of a fine discontinuity parallel to bed perpendicular joints with plumose marks. (d) SEM image (backscattered electrons micrography) of the discontinuity showing the band with voids, loose grains and increased (compared to the host rock) porosity. (e) Dilation (disaggregation) band from Nubian sandstone, Tayiba Red Beds, Sinai [from *Fossen et al.*, 2007]. The band thickness is several grain diameters.

or even after it at low σ. A similar double-part geological joint surface is presented by *Bahat et al.* [2005, Figure 6.1, p. 462]. Such features should be common in nature, but the periphery of the joint front is rarely accessible for observation.

[32] Research of the hitherto never described dilatancy band structure in natural joints certainly needs specific observations. It must be impeded by the very common aperture of joints and subsequent diagenesis (especially in carbonates) which transform the internal structure. Figure 9d shows a SEM image of a joint-parallel discontinuity (incipient joint) in Figure 9c from densely jointed Jurassic dolomicrites (fine-grained carbonate rock) of Languedoc (Figure 9b) (see *Chemenda et al.* [2011] for more details). Decohesion with porosity increase revealed by this image is similar to what is observed in GRAM 1 (Figures 8c and 8d), strongly suggesting a dilatancy band structure. Its preservation is probably made possible by the limited dissolution/

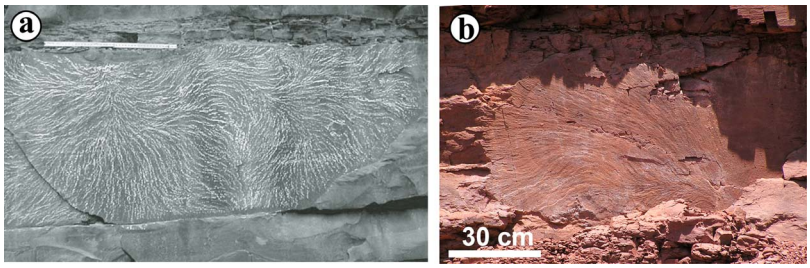

Figure 10. Plumose features on bed perpendicular natural joint surfaces. (a) In the Devonian sandstone of Ithaca Formation, Watkins Glen, New York. Scale bar is about 30 cm [*Savalli and Engelder*, 2005]. (b) In the Permian red pelites, Salagou Dam, the Lodève basin, Languedoc, southern France.

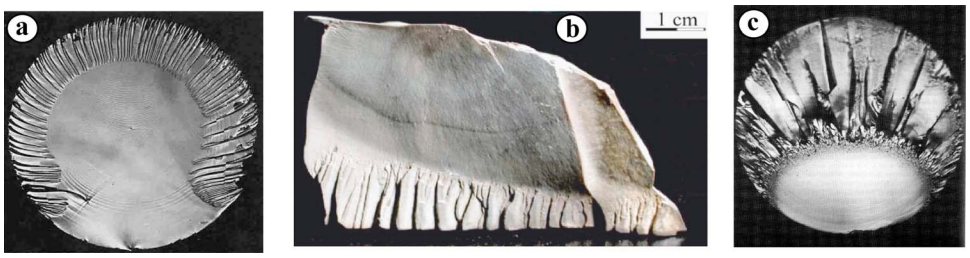

Figure 11. Aspect of hackles in glass samples and rock. (a) Fracture surface in glass rod of diameter ~1 cm broken in mixed mode I and III loading (*Sommer* [1969]; a similar result is presented by *Smekal* [1953]). (b) Jurassic limestone sample (Corconne, Hérault, France) with fringe twist hackles. (c) Fracture surface in glass rod of diameter of 4.5 mm broken in pure tension (mode I) [*Johnson and Holloway*, 1966] (a similar result is presented by *Smekal* [1953]).

precipitation process of dolomite mineral, unlike calcite carbonate rocks where dissolution/precipitation may quickly destroy the band structure and replace it with calcite infilling. Note some similarity with the dilation (disaggregation) band images of *Fossen et al.* [2007] from the Nubian sandstone of Sinaï (Figure 9e) and of *Du Bernard et al.* [2002] in poorly consolidated sands of California. (Figure 10)

[33] Thus the formation (origin) of geological joints as dilatancy bands appears to be very plausible, but as indicated, it contradicts the widely accepted view.

5.1. Arguments for Mode I Crack Mechanism and Their Critical Analysis

[34] Apart from the fact that the mode I mechanism appears as well understood within the framework of LEFM and corresponds to the orientation of natural joints in the stress space (they are orthogonal to σ_3), the principal argument in its favor is the plumose topography of joint surfaces. In other words, the same fractographic feature that was deduced from our experiments to evidence the fracture initiation as a dilatancy band (as opposed to mode I cracking) is considered as evidence of dominantly mode I origin [e.g., *Pollard et al.*, 2004]. This interpretation is based on the reading of the natural plumose patterns inspired by the LEFM [*Pollard et al.*, 1982; *Pollard and Aydin*, 1988] and by the multiaxial loading tests of glass samples [*Smekal*, 1953; *Kerkhof*, 1967; *Sommer*, 1969] interpreted in the spirit of LEFM. In these tests the initially forming (parent) mode I crack in the central part of glass rods was split into a large number of secondary twisted cracks when approaching the rod surface (Figure 11a). The resulting pattern of fringe "fracture lances" [*Kerkhof*, 1967] is similar to what is observed on some joints [e.g., *Bahat et al.*, 2005] (Figure 11b). In geological literature these features are called fringe cracks/joints or twist hackles (see, e.g., *Younes and Engelder* [1999] for terminology) and since *Smekal* [1953] and *Kerkhof* [1967] have been explained by the stress rotation resulted from mixed (I and III) mode loading along the fracture front: The secondary fractures twist during propagation to be always in mode I, i.e., orthogonal to σ_3. This seems to be generally/qualitatively true under certain conditions, although a comparison of the LFFM predictions of the twist angle values against the experimental data (mixed-mode-quasistatic loading PMMA experiments) reveals a large (up to 2 times) difference [*Cooke and Pollard*, 1996].

[35] It is of importance that the quasi-brittle fracture in both GRAM1 and mentioned above glass tests is dynamic and must be analyzed as such. Hackle fracture surfaces dynamically form in glass samples not only under mixed-mode loading but also under uniaxial extension (mode I) only [*Smekal*, 1953; *Johnson and Holloway*, 1966] (Figure 11c) (the rupture surface in Figure 11c is similar to what is sometimes observed in dynamically blasted rocks [*Bahat et al.*, 2001]).

[36] Dynamic fracture propagation was shown to result in microcracking, crack branching, and fracture surface roughening [e.g., *Lawn*, 1993] in different materials including in PMMA [e.g., *Fineberg et al.*, 1991; *Sharon and Fineberg*, 1999]. The formation of the crack surface relief is related to (but certainly not completely caused by) crack front waves [e.g., *Sharon et al.*, 2001; *Bouchaud et al.*, 2002], caused by dynamic stress transfer during crack propagation [*Willis and Movchan*, 1997]. The reality of quasi-brittle dynamic fracture in granular, frictional, cohesive, and dilatant materials is certainly even more complicated as is discussed in section 4. The plumose fractography in such materials (e.g., rocks, GRAM1) is not limited to the fringe twist hackles (in Figures 5, 6, and 10 they are not present at all). The most commonly observed features are the faint and delicate ridges ("delicate tracery of feather lines" according to the pioneering and very complete description of joints by *Woodworth* [1896]) with no systematically dominant twisting (even surfaces of the secondary fringe/twist cracks are decorated with delicate plumose [*Woodworth*, 1896; *Kulander et al.*, 1979]). These features form in the complex, essentially 3-D stress-strain field. Therefore 2-D LEFM (especially static) ignoring the material damage/microfracturing in the fracture tip process zone (PZ) does not appear to be an appropriate tool in treating quasi-brittle fracture in rock-like materials.

[37] Plumose-type fractographic features were generated in numerous tests on different materials: PMMA [e.g., *Pollard et al.*, 1982; *Bahat et al.*, 2007], starch [*Müller and Dahm*, 2000; *Müller*, 2001], metals [e.g., *Hertzberg*, 1987], glass (some papers are cited above), in single crystals [*Sherman et al.*, 2008], and in rocks [*Bahat et al.*, 2001, 2005]. Various experimentally obtained fractographic features (named striaes, lances, river patterns, cleavage steps (see, e.g., *Bahat* [1991] for terminology) have in common an aspect of diverging/elongated lineation of reliefs, but in detail they are

extremely varied and in most cases different from the delicate plumose patterns in GRAM1 and geological joints. The fractography features in different material types very likely result from different mechanisms that are subjects of intense ongoing studies in material science (there is a huge literature on the fractography of different, mostly engineering, materials, e.g., *Hull* [1999] among others). The mechanisms are not well understood but clearly depend on the material type (such as single-crystal, polycrystalline, amorphous, or granular-cohesive). Therefore geological applications should rely on the experiments on rocks and rock-type (granular-cohesive-frictional-dilatant) materials such as GRAM1. Fracture propagation velocity (static versus dynamic) and, as is shown in this paper, the normalized (by the material strength) stress values are also important.

[38] It is interesting that σ_3 orthogonal extension fractures were already obtained at compressive σ_3 long ago in rock samples [*Balsley*, 1941; *Griggs and Miller*, 1951; *Bridgman*, 1952; *Handin*, 1953; *Heard*, 1960; *Brace*, 1964]. Their origin remained obscure and was attributed to wedging or/and intrusion effects, although *Griggs and Handin* [1960] suggested that it could be related to the dynamic nature of fracturing. Curiously, after these pioneering works there were very few experimental studies of extension fracturing of rocks.

5.2. How Could Understanding Jointing Mechanisms Affect Applications?

[39] A major impact of jointing mechanisms (propagating dilatancy band versus mode I crack) refers to the prediction of spacing λ between joints, which is very important for reservoir modeling [e.g., *Committee on Fracture Characterization and Fluid Flow*, 1996]. For mode I, λ is controlled by the stress shadow effect resulting in the concept of fracture saturation [*Rives et al.*, 1992; *Bai and Pollard*, 2000a], according to which λ cannot be smaller than a certain value comparable to the layer thickness. For the localization bands, λ is defined by the stress state type and all constitutive parameters (especially by the evolution of the hardening modulus). It can vary from infinity to band thickness independent of layer thickness [*Chemenda*, 2007, 2009] (of course, in real conditions λ in a layer will be also affected by the properties of the adjacent layers and interfaces). Very dense joint sets with λ much smaller than is "allowed" by fracture saturation concepts are frequently observed in the field [i.e., *Bai and Pollard*, 2000b].

[40] Another aspect is the internal structure, the tortuosity, and the related fracture porosity contributing to the permeability increase. Within the LEFM framework [e.g., *Pollard and Aydin*, 1988], local variations in the orientation of the joint surface are considered to be caused by the variations in the orientation of the stresses: The normal to the fracture surface at each point is believed to be parallel to σ_3. The surface is conceptually considered to be well defined and corresponds to a perigranular unique planar crack [*Aydin et al.*, 2006, Figure 13]. This is very different from our experiments where, at the same (grain) scale, the joint represents a heterogeneously damaged dilatancy band with ill-defined, irregular borders that are far from being parallel on the scale of Figures 8c and 8d; see also Figure 9d). In GRAM1 experiments, every measure was taken to keep the stress field homogeneous and exclude its rotation, although we did not control the dynamic variations of the stress. The latter can trigger some variations in the orientation of the dilatancy bands at different points, but the orientation must first be related to the constitutive and stress-state parameters. A zigzag/wavy shape of localization bands similar to Figure 8c is typical for negative hardening moduli corresponding to rather brittle inelastic response of the material (see geometry of the localization bands in numerical models in Figure 12 of *Chemenda* [2009] where the stress field is practically homogeneous throughout the model).

[41] The view on fractures stemming from LEFM can be applied to rocks and rock-like materials only for very low normalized effective mean stress and at a scale much larger than the PZ size (the details of the fracture geometry/surface topography of size comparable to that of PZ are beyond the applicability of LEFM). For example, the plumose-bearing segment of the fracture surface in Figure 7a is practically orthogonal to the sample axis (itself parallel to σ_3), while the smooth segment is oriented at ~85° to the axis. This is because during manual separation of the sample resulting in a mode I crack, σ_3 was not exactly parallel to the sample axis.

[42] Note that both in GRAM1 (Figures 8c and 8d) and in dolomicrite (Figure 9d), the porosity increase within the dilatancy bands mainly occurs through the separation of the material along the grain contacts (reduction of the grain density), although transgranular microcracks are also present. In strongly cemented rocks, this can occur through any form of localized intragranular, perigranular, or cement microcracking. Low initial porosity or its complete absence should encourage this form of inelastic volume increase.

6. Conclusion

[43] The reported experimental results show that σ_3 orthogonal fractures, called in literature extension (also tensile or tension) fractures, can be of two different types resulting respectively from mode I cracking and constitutive instability in the form of dilatancy banding. The type is defined by the effective mean stress σ or its normalized value $\tilde{\sigma} = \sigma/\sigma_c$.

[44] At very small $\tilde{\sigma}$ ($\tilde{\sigma} < 0.2$), fracturing occurs through mode I cracking when the magnitude of the least tensile stress reaches a value near the tensile strength σ_t ($\sigma_3 \approx -\sigma_t$). The corresponding fracture surfaces are relatively smooth.

[45] The fractures of the second type have plumose fractography and form at higher $\tilde{\sigma}$, $0.2 < \tilde{\sigma} < 0.8$ upon meeting the yield type criterion depending on all stresses. These fractures are formed as propagating dilatancy bands. The material in the band is characterized by the heterogeneous decohesion and volume/porosity increase. The band thickness is several grain sizes. Thus fractures of this type are initially localization bands which become fractures with plumose surface after separation of the sample parts along the bands. These σ_3 orthogonal fractures/bands can form not only at tensile σ_3 but also when all stresses are compressive as long as σ_3 at banding onset does not exceed a certain positive value after which the bands become inclined to σ_1 (this occurs at $\tilde{\sigma} > 0.8$). The bands are assumed to result from the running constitutive instability where dilat-

ancy plays an important role. It is not completely clear how and why the deformation is concentrated within a narrow band, but it is suggested that it can be understood within the framework of a deformation-bifurcation approach similar to that applied to other types of deformation banding. The postbifurcation evolution and propagation of the band should be strongly related to the evolution of the constitutive parameters with the accumulated inelastic deformation. Clearly, more combined experimental, theoretical, and numerical studies are needed.

[46] The plumose fractography of fractures of the second type in GRAM1 is very similar to that of natural joints. This suggests the similarity of the formation mechanism (which is running dilatancy banding) and the name of this type of joints, the dilatancy joints. Joints forming through mode I mechanism (hence with smooth surfaces) can be called mode I joints.

[47] The results reported in this paper were obtained from axisymmetric extension tests. Axisymmetric compression and plane strain tests were also conducted and will be presented in future papers. These tests show that although the material response is sensitive to the loading configuration, the two types of fractures above form under all the loading conditions tested.

[48] **Acknowledgments.** This work results from long-term research within the framework of the Geo-FracNet consortium sponsored by SHELL and TOTAL. The authors benefited from many stimulating discussions with the industrial partners from these companies. We thank the seven reviewers and the editors for useful comments and suggestions. S. Stanchits encouraged us to present more experimental details, which made the description more complete. A. Aydin suggested a detailed comparison of our results with the traditional view on jointing in the spirit of LEFM, which has been done.

References

Aydin, A., R. I. Borja, and P. Eichhubl (2006), Geological and mathematical framework for failure modes in granular rock, *J. Struct. Geol.*, *28*, 83–98, doi:10.1016/j.jsg.2005.07.008.

Bahat, D. (1991), *Tectono-fractography*, 354 pp., Springer, Berlin.

Bahat, D., A. Rabinovitch, and V. Frid (2001), Fracture characterization of chalk in uniaxial and triaxial tests by rock mechanics, fractographic and electromagnetic radiation methods, *J. Struct. Geol.*, *23*(10), 1531–1547, doi:10.1016/S0191-8141(01)00018-9.

Bahat, D., A. Rabinovitch, and V. Frid (2005), *Tensile Fracturing in Rocks*, 569 pp., Springer, Berlin.

Bahat, D., A. Rabinovitch, V. Frid, and F. J. Brosch (2007), Cycles of subcritical tensile and shear alternating fracturing in diminishing dimensions, under tensile loading, *Int. J. Fract.*, *148*(4), 281–290, doi:10.1007/s10704-008-9201-y.

Bai, T., and D. D. Pollard (2000a), Fracture spacing in layered rocks: A new explanation based on the stress transition, *J. Struct. Geol.*, *22*, 43–57, doi:10.1016/S0191-8141(99)00137-6.

Bai, T., and D. D. Pollard (2000b), Closely spaced fractures in layered rocks: Initiation mechanism and propagation kinematics, *J. Struct. Geol.*, *22*, 1409–1425, doi:10.1016/S0191-8141(00)00062-6.

Balsley, J. R. (1941), Deformation of marble under tension at high pressure, *Eos Trans. AGU*, *22*, 519–525.

Bažant, Z. P., and J. Planas (1998), *Fracture and Size Effect in Concrete and Other Quasibrittle Materials*, CRC Press, Boca Raton, Fla.

Bésuelle, P. (2001), Compacting and dilating shear bands in porous rock: Theoretical and experimental conditions, *J. Geophys. Res.*, *106*(B7), 13,435–13,442, doi:10.1029/2001JB900011.

Bésuelle, P., and J. W. Rudnicki (2004), Localization: Shear bands and compaction bands, in *Mechanics of Fluid-Saturated Rocks*, edited by Y. Guéguen and M. Boutéca, pp. 219–321, Academic, San Diego, Calif.

Bigoni, D., and T. Hueckel (1991), Uniqueness and localization: I. Associative and non-associative elastoplasticity, *Int. J. Solids Struct.*, *28*(2), 197–213, doi:10.1016/0020-7683(91)90205-T.

Bouchaud, E., J. P. Bouchaud, D. S. Fisher, S. Ramanathan, and J. R. Rice (2002), Can crack front waves explain the roughness of cracks?, *J. Mech. Phys. Solids*, *50*, 1703–1725, doi:10.1016/S0022-5096(01)00137-5.

Brace, W. F. (1964), Brittle fracture of rocks, in *State of Stress in the Earth's Crust*, edited by W. R. Judd, pp. 111–180, Elsevier, New York.

Bridgman, P. W. (1952), *Studies in Large Plastic Flow and Fracture*, 362 pp., McGraw-Hill, New York.

Chemenda, A. I. (2007), The formation of shear-band/fracture networks from a constitutive instability: Theory and numerical experiment, *J. Geophys. Res.*, *112*, B11404, doi:10.1029/2007JB005026.

Chemenda, A. I. (2009), The formation of tabular compaction-band arrays: Theoretical and numerical analysis, *J. Mech. Phys. Solids*, *57*, 851–868, doi:10.1016/j.jmps.2009.01.007.

Chemenda, A. I. (2011), Origin of compaction bands: Anti-cracking or constitutive instability?, *Tectonophysics*, *499*, (1–4), 156–164, doi:10.1016/j.tecto.2011.01.005.

Chemenda, A. I., S.-H. Nguyen, J.-P. Petit, and J. Ambre (2011), Experimental evidences of transition from mode I cracking to dilatancy banding, *C. R. Mec.*, doi:10.1016/j.crme.2011.01.002, in press.

Committee on Fracture Characterization and Fluid Flow (1996), *Rock Fractures and Fluid Flow: Contemporary Understanding and Applications*, Natl. Res. Counc., Washington, D. C.

Cooke, M. L., and D. D. Pollard (1996), Fracture propagation paths under mixed mode loading within rectangular blocks of polymethyl methacrylate, *J. Geophys. Res.*, *101*(B2), 3387–3400, doi:10.1029/95JB02507.

Du Bernard, X., P. Eichhubl, and A. Aydin (2002), Dilation bands: A new form of localized failure in granular media, *Geophys. Res. Lett.*, *29*(24), 2176, doi:10.1029/2002GL015966.

Fineberg, J., S. P. Gross, M. Marder, and H. L. Swinney (1991), Instabilities in dynamic fracture, *Phys. Rev. Lett.*, *67*, 457–460, doi:10.1103/PhysRevLett.67.457.

Fossen, H., R. A. Schultz, Z. K. Shipton, and K. Mair (2007), Deformation bands in sandstone: A review, *J. Geol. Soc.*, *164*(4), 755–769, doi:10.1144/0016-76492006-036.

Griffith, A. A. (1924), Theory of rupture, in *Proceedings of the First International Congress for Applied Mechanics*, edited by C. B. Biezeno and J. M. Burges, pp. 55–63, Int. Union of Theor. and Appl. Mech., Delft., Netherlands.

Griggs, D., and J. Handin (1960), Observations on fracture and a hypothesis of earthquakes, in *Rock Deformation*, vol. 79, edited by D. Griggs and J. Handin, pp. 347–364, Geol. Soc. of Am., Boulder, Colo.

Griggs, D., and W. B. Miller (1951), Deformation of Yule marble, Part I, *Geol. Soc. Am. Bull.*, *62*(8), 853–862, doi:10.1130/0016-7606(1951)62[853:DOYMPI]2.0.CO;2.

Handin, J. (1953), An application of high pressure in geophysics: Experimental rock deformation, *Am. Soc. Mech. Eng. Trans.*, *75*, 315–324.

Heard, H. C. (1960), Transitions from brittle fracture to ductile flow in Solenhofen limestone as a function of temperature, confining pressure and interstitial fluid pressure, in *Rock Deformation*, vol. 79, edited by D. Griggs and J. Handin, pp. 193–226, Geol. Soc. of Am., Boulder, Colo.

Hertzberg, R. W. (1987), Fracture surface micromorphology in engineering solids, in *Fractography of Modern Engineering Materials: Composites and Metals*, edited by J. E. Masters and J. J. Au, pp. 5–32, ASTM Int., Philadelphia, Pa., doi:10.1520/STP25613S.

Hillerborg, A., M. Modéer, and P.-E. Petersson (1976), Analysis of crack formation and crack growth in concrete by means of fracture mechanics and finite elements, *Cement Concr. Res.*, *6*(6), 773–781, doi:10.1016/0008-8846(76)90007-7.

Hull, D. (1999), *Fractography: Observing, Measuring and Interpreting Fracture Surface Topography*, 366 pp., Cambridge Univ. Press, New York.

Issen, K. A., and J. W. Rudnicki (2000), Conditions for compaction bands in porous rocks, *J. Geophys. Res.*, *105*, 21,529–21,536, doi:10.1029/2000JB900185.

Johnson, J. W., and D. G. Holloway (1966), On the shape and size of the fracture zones on glass fracture surfaces, *Philos. Mag.*, *14*(130), 731–743, doi:10.1080/14786436608211968.

Kerkhof, F. (1967), Sprödbruchmodulation durch elastisch Wellen, in *Kurzzeitphysik*, edited by K. Vollrath and G. Thomer, pp. 498–552, Springer, New York.

Kulander, B. R., C. C. Barton, and S. L. Dean (1979), The application of fractography to core and outcrop fracture investigations, *Rep. METC/SP-79/3*, 174 pp., Morgantown Energy Technol. Cent., Morgantown, W. Va.

Lawn, B. (1993), *Fracture of Brittle Solids*, 2nd ed., 378 pp., Cambridge Univ. Press, New York, doi:10.1017/CBO9780511623127.

Mandl, G. (2005), *Rock Joints. The Mechanical Genesis*, 212 pp., Springer, New York.

McClintock, F. A., and G. R. Irwin (1965), Plasticity aspects of fracture mechanics, in *Fracture Toughness Testing and Its Applications*, pp. 84–113, ASTM Int., Philadelphia, Pa.

Müller, G. (2001), Experimental simulation of joint morphology, *J. Struct. Geol.*, *23*(1), 45–49, doi:10.1016/S0191-8141(00)00104-8.

Müller, G., and T. Dahm (2000), Fracture morphology of tensile cracks and rupture velocity, *J. Geophys. Res.*, *105*(B1), 723–738, doi:10.1029/1999JB900314.

Nguyen, S.-H., A. I. Chemenda, and J. Ambre (2011), Influence of the loading conditions on the mechanical response of granular materials as constrained from experimental tests on synthetic rock analogue material, *Int. J. Rock Mech. Min. Sci.*, *48*, 103–115.

Ottosen, N. S., and K. Runesson (1991), Properties of discontinuous bifurcation solutions in elasto-plasticity, *Int. J. Solids Struct.*, *27*, 401–421, doi:10.1016/0020-7683(91)90131-X.

Perrin, G., and J. B. Leblond (1993), Rudnicki and Rice's analysis of strain localization revisited, *J. Appl. Mech.*, *60*, 842–846, doi:10.1115/1.2900992.

Petersson, P. E. (1981), Crack growth and development of fracture zones in plain concrete and similar materials, *Rep. TVBM–1006*, Div. Build. Mat., Lund Inst. of Technol., Lund, Sweden.

Pollard, D. D., and A. Aydin (1988), Progress in understanding jointing over the past century, *Bull. Geol. Soc. Am.*, *100*, 1181–1204, doi:10.1130/0016-7606(1988)100<1181:PIUJOT>2.3.CO;2.

Pollard, D. D., P. Segall, and P. T. Delaney (1982), Formation and interpretation of dilatant echelon cracks, *Geol. Soc. Am. Bull.*, *93*(12), 1291–1303, doi:10.1130/0016-7606(1982)93<1291:FAIODE>2.0.CO;2.

Pollard, D. D., S. Bergbauer, and I. Mynatt (2004), Using differential geometry to characterize and analyse the morphology of joints, in *The Initiation, Propagation, and Arrest of Joints and Other Fractures*, vol. 231, edited by J. W. Cosgrove and T. Engelder, pp. 153–182, J. Geol. Soc. London, London.

Reches, Z., and D. A. Lockner (1994), Nucleation and growth of faults in brittle rocks, *J. Geophys. Res.*, *99*(B9), 18,159–18,173, doi:10.1029/94JB00115.

Reynolds, O. (1885), On the dilatancy of media composed of rigid particles in contact, with experimental illustrations, *Philos. Mag.*, *20*(5), 469–481.

Rice, J. R. (1968), Mathematical analysis in the mechanics of fracture, in *Fracture: An Advanced Treatise*, vol. 2, edited by H. Liebowitz, chap. 3, pp. 191–311, Academic, New York.

Rice, J. R. (1973), The initiation and growth of shear bands, in *Plasticity and Soil Mechanics*, edited by A. C. Palmer, pp. 263–274, Cambridge Univ. Press, Cambridge, U. K.

Rice, J. R. (1976), The localization of plastic deformation, in *Theoretical and Applied Mechanics*, vol. 1, edited by W. T. Koiter, pp. 207–220, North-Holland, New York.

Rives, T., M. Razack, J.-P. Petit, and K. D. Rawnsley (1992), Joint spacing: Analogue and numerical simulations, *J. Struct. Geol.*, *14*(8–9), 925–937, doi:10.1016/0191-8141(92)90024-Q.

Rudnicki, J. W., and J. R. Rice (1975), Conditions for the localization of deformation in pressure-sensitive dilatant materials, *J. Mech. Phys. Solids*, *23*(6), 371–394, doi:10.1016/0022-5096(75)90001-0.

Savalli, L., and T. Engelder (2005), Mechanisms controlling rupture shape during subcritical growth of joints in layered rocks, *Geol. Soc. Am. Bull.*, *117*(3), 436–449, doi:10.1130/B25368.1.

Sharon, E., and J. Fineberg (1999), The dynamics of fast fracture, *Adv. Eng. Mater.*, *1*(2), 119–122, doi:10.1002/(SICI)1527-2648(199910)1:2<119::AID-ADEM119>3.0.CO;2-2.

Sharon, E., G. Cohen, and J. Fineberg (2001), Propagating solitary waves along a rapidly moving crack front, *Nature*, *410*, 68–71, doi:10.1038/35065051.

Sherman, D., M. Markovitz, and O. Barkai (2008), Dynamic instabilities in {1 1 1} silicon, *J. Mech. Phys. Solids*, *56*(2), 376–387, doi:10.1016/j.jmps.2007.05.010.

Smekal, A. G. (1953), Zum Bruchvorgang bei sprödem Stoffverhalten unter ein– und mehrachsigen Beanspruchungen, *Oesterr. Ing. Arch.*, *7*, 7–49.

Sommer, E. (1969), Formation of fracture lances in glass, *Eng. Fract. Mech.*, *1*(3), 539–546, doi:10.1016/0013-7944(69)90010-1.

Sulem, J., and H. Ouffroukh (2006), Shear banding in drained and undrained triaxial tests on a saturated sandstone: Porosity and permeability evolution, *Int. J. Rock Mech. Min. Sci.*, *43*, 292–310, doi:10.1016/j.ijrmms.2005.07.001.

Van Mier, J. G. M. (1997), *Fracture Processes of Concrete: Assessment of Material Parameters for Fracture Models*, 448 pp., CRC Press, Boca Raton, Fla.

Vardoulakis, I., and J. Sulem (1995), *Bifurcation Analysis in Feomechanics*, 462 pp., Blackie, New York.

Willis, J. R., and A. B. Movchan (1997), Three dimensional dynamic perturbation of a propagating crack, *J. Mech. Phys. Solids*, *45*(4), 591–610, doi:10.1016/S0022-5096(96)00102-0.

Wong, T.-F. (1982), Shear fracture energy of Westerly granite from post-failure behavior, *J. Geophys. Res.*, *87*, 990–1000, doi:10.1029/JB087iB02p00990.

Wong, T.-F., C. David, and W. Zhu (1997), The transition from brittle faulting to cataclastic flow in porous sandstones: mechanical deformation, *J. Geophys. Res.*, *102*, 3009–3025, doi:10.1029/96JB03281.

Woodworth, J. B. (1896), The fracture system of joints, with remarks on certain great fractures, *Boston Natl. Hist. Proc.*, *27*, 163–183.

Younes, A. I., and T. Engelder (1999), Fringe cracks: Key structures for the interpretation of the progressive Alleghanian deformation of the Appalachian plateau, *Geol. Soc. Am. Bull.*, *111*(2), 219–239, doi:10.1130/0016-7606(1999)111<0219:FCKSFT>2.3.CO;2.

J. Ambre and A. Chemenda, Géoazur, Université de Nice-Sophia Antipolis, CNRS, 250 Rue Albert Einstein, F-06560 Valbonne, France. (chem@geoazur.unice.fr)

S.-H. Nguyen, Department of Project Management, Academy of Managers for Construction and Cities, Ministry of Construction, 37 Le Dai Hahn St., Hanoi, Vietnam.

J.-P. Petit, Géosciences Montpellier, Université Montpellier 2, Place E. Bataillon, F-34095 Montpellier CEDEX 5, France.